ADVANCED FUNCTIONAL MATERIALS
www.afm-journal.de

Accurate and Reliable Detection of Dynamic Electrophysiological Signals via In Situ Formation of Epidermal Electrodes

Chubin He, Jing Zhang, Haifei Wang, Di Wu, Haoyu Zheng, Zhenan Guo, Juan Xie, Wanhong Zhu, Moyi Xie, Jun Zhong, Yongfeng Liu, Zihao Li, Guanhua Lin, and Zhengchun Peng**

Accurate and reliable monitoring of dynamic electrophysiological signals is essential for advancing human health. However, gaps and relative movements between the detection electrodes and human skin can severely interfere the accuracy and stability of acquired bioelectrical signals. Here, an approach to rapidly form a stable bioelectronic interface through an in situ self-catalytic reaction at the interface between an organogel electrode and the epidermal tissue of skin, referred to as the epidermisgel interlocking electrode (EGIE), is proposed. Significantly, the electrode with an interlocking structure exhibits superior interfacial adhesion, excellent epidermal conformability, outstanding mechanical stability, stable electrochemical performance, and good biocompatibility. Accurate and reliable detection of electrocardiogram (ECG) signals during walking, squatting, jogging, and post-sweating, as well as electromyogram (EMG) signals during leg stretching exercises and running activities, is achieved with a signal-to-noise ratio of 21.83 ± 0.12 dB. An EGIE-enabled ECG wear is further developed for multi-parameter physiological monitoring during dynamic human activities, which demonstrates the promising application of the proposed method.

1. Introduction

With the development of wearable health monitoring devices and smart medical technologies for human health, the demand for real-time, long-term dynamic monitoring of bioelectrical signals is surging.[1] Notably, the reliability, stability, comfort, and personalization of these devices are also critical for monitoring bioelectrical signals from people, due to interferences from body movements, sweat, and other physiological factors.[2] Therefore, developing highly compatible, effective, and comfortable wearable health monitoring devices for gaining reliable bioelectronic signals is necessary, and becomes one of the most daunting challenges in modern science and technology.[3] In order to establish bioelectronic communication between human tissues and external electronic devices, biocompatible electrodes have been the most commonly used terminals.[3a] During usage of these electrodes, two interfaces play a key role, one is the biological interface between tissues and electrodes, which is used to transmit the potential difference signal generated by tissue stimulation. The other is the physical connection interface between the electrode and the external device, which is used to record the characteristic signals from the physiological activities. To build an excellent bioelectronic interface, the electrode material needs

C. He, J. Zhang, H. Wang, D. Wu, H. Zheng, Z. Guo, J. Xie, W. Zhu, Z. Peng
State Key Laboratory of Radio Frequency Heterogeneous Integration
College of Physics and Optoelectronic Engineering
Shenzhen University
Shenzhen 518060, China
E-mail: zcpeng@szu.edu.cn

M. Xie, G. Lin
Strait Laboratory of Flexible Electronics (SLoFE)
Fujian Key Laboratory of Flexible Electronics
Strait Institute of Flexible Electronics (SIFE Future Technologies)
Fujian Normal University
Fuzhou 350117, China
E-mail: lingh@fjnu.edu.cn

J. Zhong, Y. Liu
Suzhou Institute of Biomedical Engineering and Technology
Chinese Academy of Science
Suzhou 215163, China

Z. Li, Z. Peng
School of Electronic Information and Electrical Engineering
Shanghai Jiao Tong University
Shanghai 200240, China

The ORCID identification number(s) for the author(s) of this article can be found under https://doi.org/10.1002/adfm.202509372

DOI: 10.1002/adfm.202509372

to meet the requirements of fine conductivity, low interface impedance, and high tissue adhesion[4] and has excellent epidermal conformability, mechanical stability, and biocompatibility with tissue.[5]

In recent years, significant achievements have been made in overcoming the limitations of traditional electrodes for physiological signal detection through material design and structural optimization.[6] For the material optimization, advanced materials such as metal nanomaterials,[7] conductive polymers,[8] and their composites[9] have demonstrated exceptional conductivity and tunable doping properties, making them ideal for flexible epidermal biosensors. These materials enable high-precision electrophysiological monitoring.[10] For instance, Hyeokjun Yoon et al. developed a controllable patterning technique for metal nanowires (e.g., Ag, Ag@Au core-shell, and Ag@(Au-Pt) on electrospun nanofiber membranes, creating stretchable, breathable, and highly conductive epidermal devices for epicardial signal recording, biosensing, and customized electromyography.[11] However, such electrodes remain vulnerable to sweat-induced contact impedance changes, which degrade signal quality.[12] For the electrode structure design, efforts to enhance electrode design have focused on engineered architectures[13] and microneedle arrays,[14] which show significant advantages in real-time monitoring and long-term wearing scenarios.[15] For example, Jeong et al. reported a stretchable microneedle adhesive patch with superior skin permeability and electromechanical stability for reliable electrophysiological (EP) signal acquisition across diverse skin conditions.[16] It should be noted that this minimally invasive electrode needs to penetrate the surface of the skin, which may cause discomfort or infection risks.[14a,17] Despite many advantages, microneedle-based systems still face challenges, including complex fabrication, potential skin irritation, and infection risks, which compromise user comfort. In addition, most of the current electrode materials only achieve stable and reliable monitoring signals under static condition by improving flexibility, skin conformability, conductivity, and self-adhesion, due to the reduction of interface impedance and minimization of environmental noise and motion artifacts.[18] However, for real-time monitoring of electrophysiological signals during complex dynamic movements, there is still an enormous challenge to set up the tissue-electrode-device connection loop through material design and preparation technology for building an excellent bioelectronic interface to acquire stable, high-quality electrophysiological (EP) signals. This challenge is particularly acute in wearable health devices, where reliable dynamic signal monitoring is both technologically demanding and clinically essential for advancing personalized healthcare.

Herein, we present a novel approach to in situ form a stable bioelectronic interface between a conductive gel electrode and human tissue, referred to as the epidermis-gel interlocking electrode (EGIE) (**Figure 1a**), which is rapidly formed by a gel precursor with a certain viscosity painted onto the epidermal tissue. Under a self-catalytic reaction, a stable interlocking structure is formed at the interface between the gel electrode and the epidermal tissues. These EGIEs can ensure superior conformability to epidermal tissue, minimizing motion artifacts caused by relative displacement during movement, low interfacial impedance ensuring high signal fidelity, excellent mechanical stability, strong dynamic adhesion, stable electrochemical performance for reliable long-term use, and outstanding biocompatibility. As such, the EGIE can collect ECG and EMG signals with improved signal-to-noise ratio (SNR) and stability during dynamic motion. We demonstrate the significant application of our EGIE by integrating it into smart clothes for long-term monitoring of multiple physiological parameters under various human motions.

2. Results and Discussion

2.1. Design and In Situ Formation of Epidermis-Gel Interlocking Electrode (EGIE)

The EGIE was formed by an organogel undergoing in situ self-catalytic reaction to create an interlocking structure with the epidermal tissue. The organogel framework consisted of a copolymer network of 2-acrylamido-2-methyl-1-propanesulfonic acid (AMPS), [2-(methacryloloxy) ethyl] dimethyl-(3-sulfopropyl) (MAEDS), and acrylamide (AAm) (Figure 1b). The poly-AAm chains provided elastic mechanical properties and structural stability, while the polyelectrolytes poly-AMPS and poly-MAEDS, containing both positively and negatively charged groups as well as hydrophobic functional groups, endow the organogel with excellent ionic conductivity and adhesion properties. Owing to the use of citric acid and sorbitol as supramolecular solvent components, the carboxyl and hydroxyl groups in these molecules formed extensive hydrogen bonds upon dissolution in water, which could simultaneously enhance solution's viscosity and maintain the precursor solution's permeability. This process provided the essential basis for forming the bio-interfacial interlocking structure on the epidermis. Besides, non-covalent interactions (e.g., hydrogen bonds, electrostatic forces) within the supramolecular solvent further reinforced the gel's mechanical robustness. Moreover, silver ions (Ag^+) were employed as the catalyst for gel formation. The inclusion of Ag^+ effectively activated ammonium persulfate (APS) and accelerated radical generation, consequently enable rapid in situ polymerization of vinyl-functional monomers within seconds to minutes.[18b,c] Experimental observations showed that precursor solutions containing Ag^+ have a much faster speed for the formation of gels than solutions without Ag^+ (Figure S1, Supporting Information), illustrating that the APS supramolecular solution with silver nitrate can fastly generate sufficient free radicals to initiate the self-polymerization of the organogel under ambient conditions. To further verify their rapid gelation, we dropped the gel precursor onto a PET film and displayed the reaction state at different reaction times (Figure 1c). At the beginning, the precursor was in a solution state and flowed easily. After 1 min of reaction, the viscosity of the solution increased, leading to the generation of filamentous polymers when the solution pulled up. Only 4 min later, the solution was changed from a semi-gel state (3 min) to an adhesive gel state (5 min). These results demonstrated that the gel precursor solution could spontaneously conduct the polymerization reaction and quickly form a stable adhesive interface at room temperature, thanks to the functions of the supramolecular solvent and the catalytic effect of Ag^+ ions.

Leveraging the rapid autocatalytic crosslinking, EGIE precursors can be directly patterned onto complex biological surfaces via brush-painting or syringe-injection, enabling customized electrode geometry at desired locations on the human body.

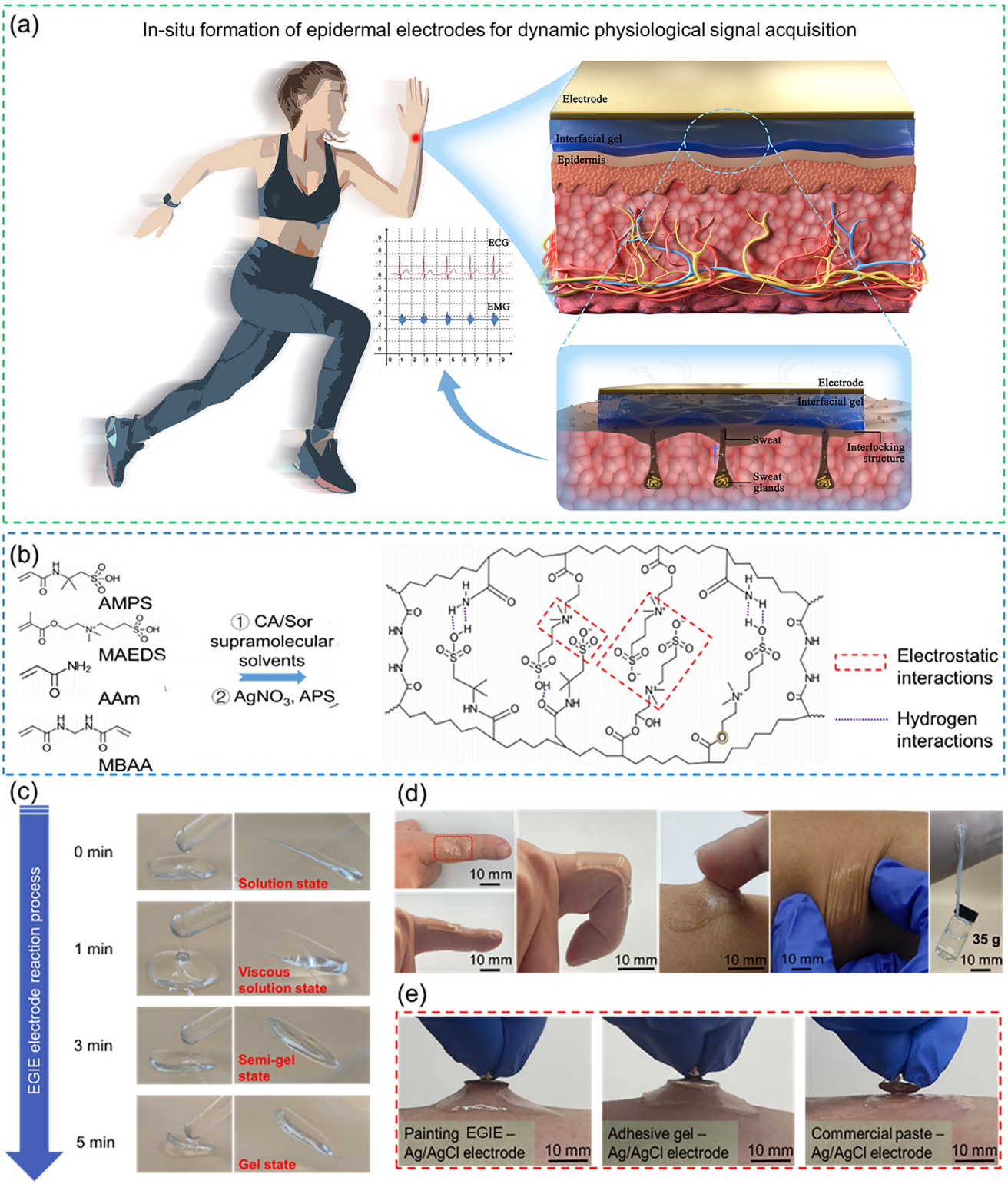

Figure 1. Design and Formation of EGIE. a) Schematic of dynamic detection electrophysiological signals for EGIE electrode (the permission to use the image is obtained). b) Structure of the organogel. c) Photographs of direct painting gel precursor on PET film and in situ gelation on skin after 5 min. d) a conformal EGIE with human skin. e) Photographs showing the superior attachment of button electrodes with different gel interfaces.

Surprisingly, the painted precursor spontaneously underwent gelation in less than 5 min and formed an epidermal electrode with robust mechanical strength and excellent adhesion to skin (Figures S2 and Movie S1, Supporting Information). Even under complex mechanical deformations such as bending the finger 90°, stretching, compressing, twisting, and lifting heavy objects, no noticeable crevice was observed between the electrode and skin (Figure 1d). Besides, EGIE can seamlessly interact with the Ag/AgCl electrode due to the in situ gelation. As shown in Figure 1e, the EGIE could anchor the Ag/AgCl electrode to skin surface without requiring any additional physical fixation. This dual-interface optimization enables robust electrical connections throughout the bioelectronic system, successfully circumventing the delamination issue in the traditional metal-hydrogel system. These results suggest that the EGIE can be used to build reliable bioelectronic interface on human skin for high-fidelity acquisition of physiological signals, such as ECG and EMG.

2.2. Mechanical and Interfacial Properties of the Epidermal-Gel Interlocking Electrode (EGIE)

Generally, an epidermal electrode should meet several requirements for achieving dynamic monitoring. First, the elastic modulus and extensibility of the EGIE should match human skin (≈10–100 kPa, >50% strain) to ensure conformal contact and minimize detachment risks.[19] Second, the EGIE require excellent mechanical stability, particularly in terms of anti-creep performance, low stress relaxation, and fatigue resistance, to maintain interfacial integrity during prolonged dynamic activity.[20] Thirdly, strong adhesion prevents slippage and reduces motion artifacts, requiring a balance between cohesive energy and surface bonding.[21] In this work, we regulated the coexistence of mechanical properties and interfacial adhesion performance of the EGIE by introducing an elastic polymer network.

Figure 2a shows the stress-strain curves of EGIE with varying acrylamide (AAm) concentration. By modulating AAm concentration, the elastic modulus of the IEGIE was tunable from 8.97 ± 4.1 kPa (1379.52 ± 150.2% fracture strain) to 42.63 ± 4.1 kPa (≈900 ± 132% strain), spanning the mechanical range of epidermal tissue (Figure 2b). Besides, the introduction of elastic poly-AAm network could endow the EGIE with a reversible stretchability up to 300% (Figure 2c) and rate-dependent mechanical adaptability (Figure S3, Supporting Information), as high stretchability of the EGIE is critical for reducing the risk of delamination, maintaining dynamical stability of electrode-skin interfaces, and long-term use. In addition, the adhesion strength of the EGIE was investigated through varying AAm content by 180-degree peel tests. The results showed that the adhesion strength peaked at 175 ± 4.5 N/m for a MAEDS: AMPS: AAm molar ratio of 1:1:3 (Figure 2d). Lower AAm content weakened cohesion, while higher content enhanced energy dissipation via hydrogen bonding, electrostatic interactions, and hydrophobic associations,[22] which can increase the interfacial toughness and improve the adhesion performance of the EGIE. Herein, the molar ratio of MAEDS: AMPS: AAm has been fixed at 1:1:3 to prepare EGIEs for achieving excellent comprehensive performances in our investigations.

It was worth noting that the addition of $AgNO_3$ markedly improved the adhesion strength of the IEGIE to ≈310 ± 15.2 N m^{-1} (Figure 2e). This phenomenon could be attributed to the following factors. First, Ag^+ ions catalyzed rapid polymerization, fostering a densely crosslinked 3D network with robust structural integrity.[18b,23] Second, the introduction of $AgNO_3$ could enhance the hydrogen bonding, ionic interactions, and van der Waals interactions between the EGIE and human skin,[24] thus improving surface affinity of the EGIE. Beside, we tested the interfacial adhesion of EGIE electrodes to the skin using a 90° peel test (Figure 2f). The adhesion properties of the EGIE electrode to the skin are enhanced by ≈50% over commercial pastes and adhesive gel electrodes. The superior interfacial adhesion of EGIE was highly beneficial for detecting physiological signals, as it greatly facilitated the conformality between the EGIE electrode and the epidermis. Besides, the EGIE exhibited exceptional stability in storage and repeated usages. No significant reduction of performance was observed even after 700 attachment/detachment cycles (Figure S4, Supporting Information), and the EGIE can maintain its adhesion strength for 14 days at room temperature (Figure S5, Supporting Information). Additionally, the adhesion force of the EGIE-Ag-film interface was more than twice that of commercial conductive pastes (Figure S6, Supporting Information). The strong GELE-Ag adhesion interactions allow overcoming the traditional metal-hydrogel delamination challenges for achieving excellent signal stability.

Moreover, the EGIE possess excellent anti-creep properties and still maintains stable mechanical strain, under 0.2 N tensile loading for 12 h (Figure 2g). In contrast, PMA gels exhibited a rapid increase in mechanical strain after 6000 s of loading and fractured at ≈10 000 s. Similarly, the EGIE sustained tensile stress for nearly 40 000 s under 100% strain (Figure S7, Supporting Information). Compared with PMA gels, the EGIE showed only a 10% reduction in stress, indicating significantly lower stress relaxation. Additionally, cyclic tensile tests of EGIE under different strains and tensile rates for 1000 cycles revealed stable strength retention (Figure 2h; Figure S8, Supporting Information). These results demonstrated excellent mechanical stability and fatigue resistance of the EGIE, attributed to the formation of an elastic poly-AAm copolymer network within EGIE.

Furthermore, the EGIE also demonstrated exceptional biocompatibility. When adhered to the epidermis, the EGIE could be firmly attached without causing redness or allergic reactions, up to seven days (Figure 2i), which also demonstrates that these EGIEs do not interfere with normal skin perspiration, as no adverse reactions (e.g., redness or swelling) were observed on skin. Besides, we rigorously evaluated EGIE's biocompatibility through in vitro cytotoxicity testing. Confocal microscopy images clearly demonstrated that the L929 cells in EGIE exhibited comparable viability to those in control group (Figure S9a, Supporting Information). And, the L929 cell viability remains >99% after 144-h exposure to EGIE measured by the methyl thiazolyl tetrazolium (MTT) assay (Figure S9b, Supporting Information), indicating their nontoxic nature. Interestingly, the EGIE can be easily detached from skin by ethanol treatment, and the adhesion performance is restored once the ethanol evaporated (Figure S10, Supporting Information), which show great application prospects in the field of medical diagnosis and treatment. We proposed the potential mechanism of ethanol-mediated

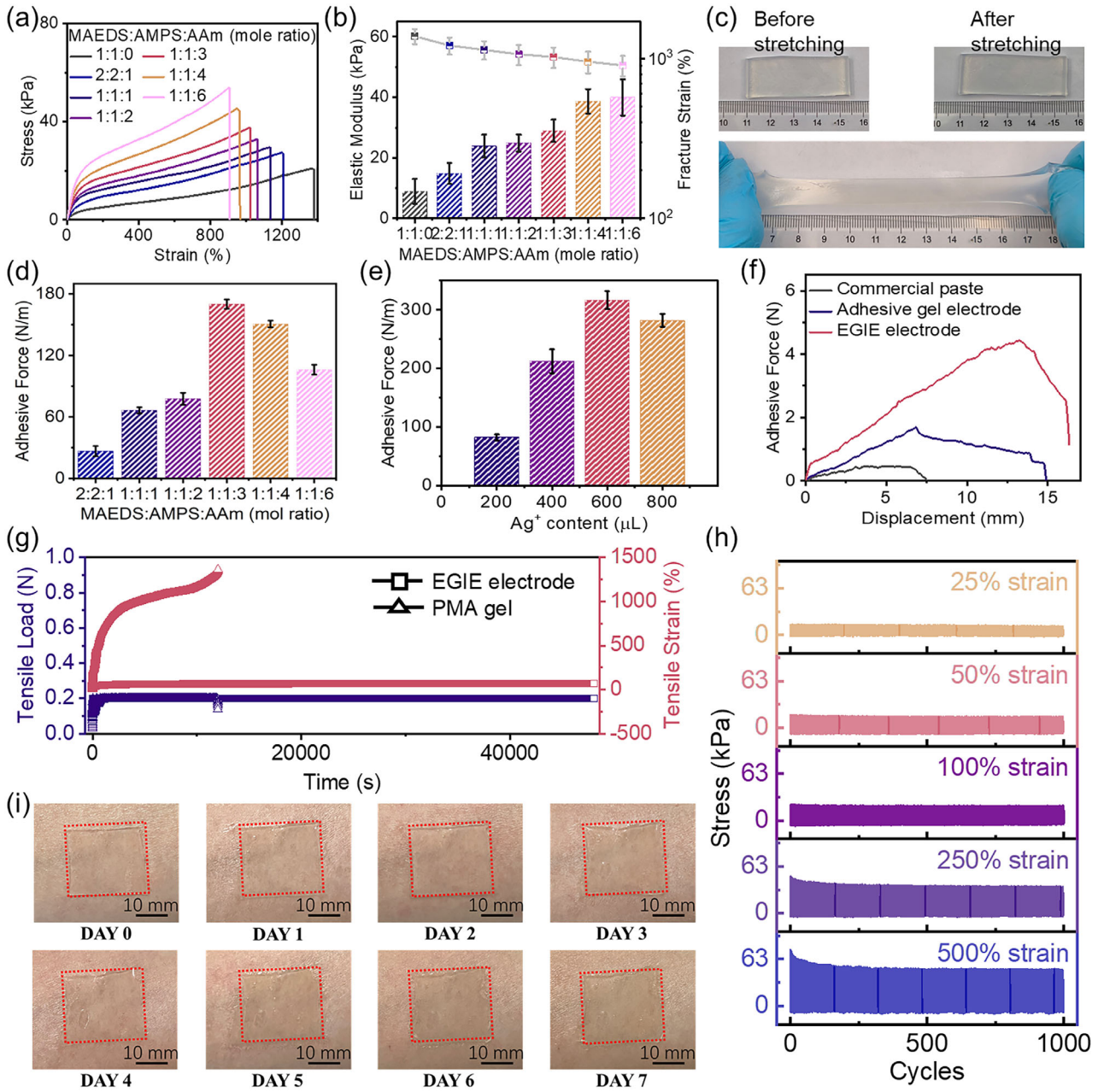

Figure 2. Mechanical and Interfacial Properties of EGIE. a) Stress–strain curves, b) Elastic modulus, and fracture strain of the EGIE with different MAEDS:AMPS:AAm mole ratio. c) Images of the EGIE presenting little residual strain even after being stretched to 300% of strain. d) The adhesive force of the EGIE with different MAEDS:AMPS:AAm mole ratio. e) The adhesive force of the EGIE with different $AgNO_3$ content. f) The interfacial adhesion of different electrodes to the skin. g) The anti-creep properties of the EGIE. h) Cyclic tensile tests of the EGIE under varying strains. i) Photographs of the EGIE on skin with 7 days. Data in (C) and (D) are means ± SD, $n = 3$.

detachment: 1) ethanol may modulate the surface energy at the EGIE-skin interface, consequently reducing adhesive forces; 2) as shown in Figure S11a (Supporting Information), ethanol residues can form an insulating interfacial layer that prevents direct electrode-skin contact, thereby diminishing adhesion. Furthermore, the ethanol-mediated detachment process causes no adverse effects on skin tissue, as no observed erythema or other physiological reactions (Figure S11b and Movie S2, Supporting Information).

2.3. Electrochemical Properties of the Epidermal-Gel Interlocking Electrode (EGIE)

The electrochemical properties of EGIE were systematically characterized to evaluate its efficacy as a bioelectronic interface for high-fidelity signal transmission. Electrochemical impedance spectroscopy (EIS) revealed that ionic conductivity of EGIE could be precisely modulated by varying acrylamide (AAm) content (**Figure** 3a; Figure S12, Supporting Information). Compared

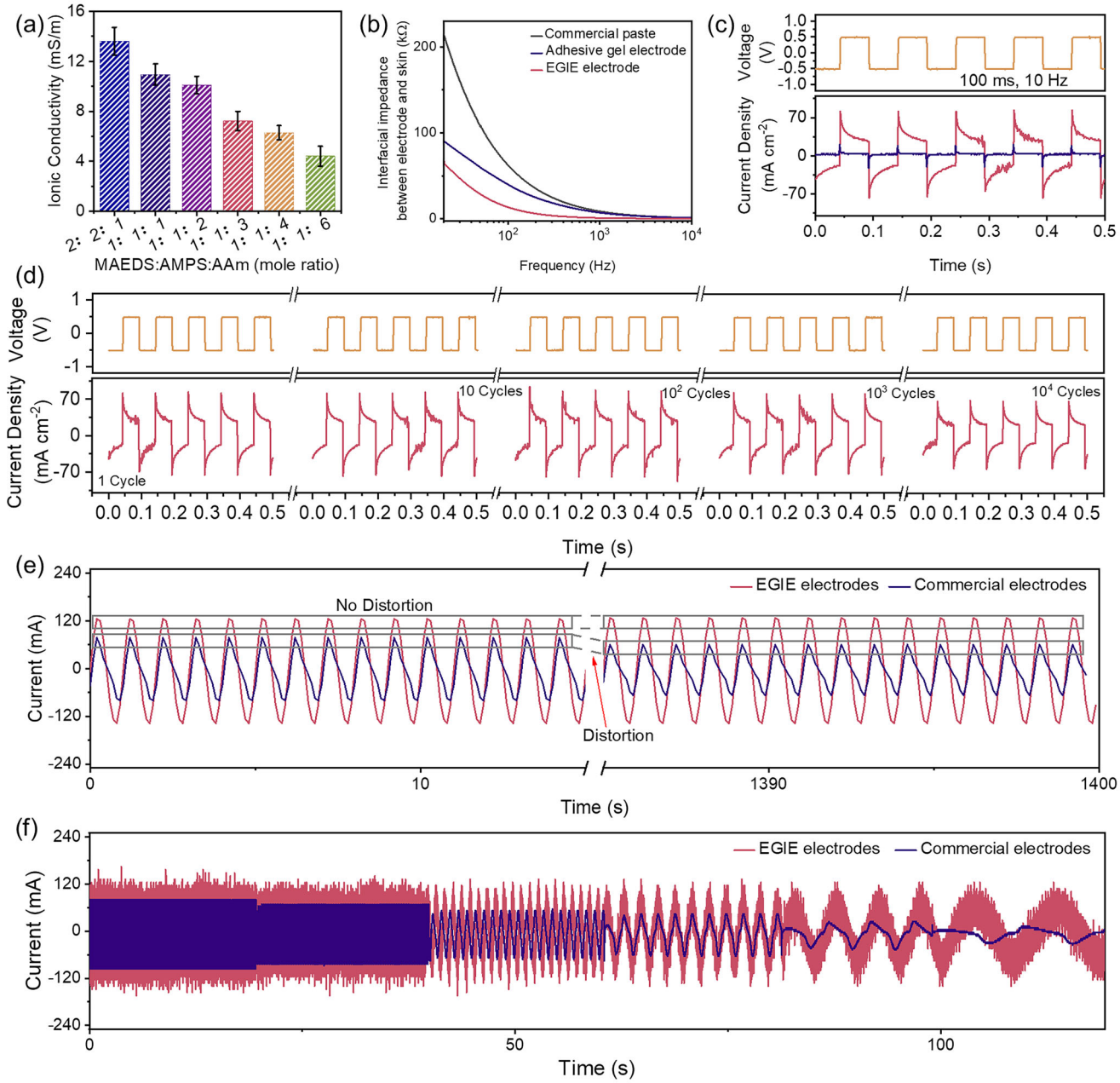

Figure 3. Electrochemical Properties of EGIE. a) The ionic conductivity of EGIE with different MAEDS:AMPS:AAm molar ratios. b) The interfacial impedance between electrodes and skin with different electrodes. c) The current density of the EGIE and commercial Ag/AgCl electrodes with biphasic pulse electrical stimulation at 10 Hz and ±500 mV. Red is the EGIE, and Blue is the commercial Ag/AgCl electrode. d) The electrical performance of the EGIE after 10000 cycles biphasic pulse electrical stimulation. e) The electrical performance of the EGIE applied 10 Hz, 0.5 V sinewave pulse 1400 cycles. f) The electrical performance of the EGIE under sinewave stimulation at different frequencies from 10 to 0.1 Hz. Data in (G) are means ± SD, $n = 3$.

with recently reported gel electrodes, the EGIEs possess superior impedance performance (<450 ± 2.8 Ω) at physiologically relevant frequencies.[25] Moreover, we tested the interfacial impedance between different electrodes and the skin, and the results showed that the EGIE exhibited ≈25% lower electrode-skin impedance than commercial pastes and adhesive gel electrodes (Figure 3b), leading to high-fidelity signal acquisition. Furthermore, the impedance value of the EGIEs was decreased with the reduction in thickness (Figure S13, Supporting Information), but their ionic conductivity was increased as the temperature improved from −15 °C to 90 °C (Figure S14, Supporting Information). To evaluate their dynamic detection capability for physiological signals, we performed the biphasic pulse testing on the EGIEs to further characterize their interfacial electrochemical performance. These EGIEs could generate higher injection current density of approximately ≈81.52 ± 0.89 mA cm^{-2} compared to the commercial Ag/AgCl electrodes (≈20.38 ± 0.52 mA cm^{-2}) at 10 Hz and ±500 mV biphasic pulse electrical

stimulation (Figure 3c), which indicates that the EGIEs have lower interfacial impedance performance. Moreover, the EGIE maintained stable electrical performance (Figure 3d) even after 10000 charge-discharge cycles. And these EGIEs also have stable electrical signal output performance during biphasic pulse testing at various frequencies (Figure S15, Supporting Information). When a 10 Hz, 0.5 V sinusoidal pulse was applied, the IEGIE electrode maintained stable performance without signal attenuation or distortion after 1400 cycles (Figure 3e). In contrast, commercial gel electrodes exhibited the performance degradation under identical testing conditions. These results highlighted their practical applications owing to the exceptional durability and electrical performance of the EGIEs during prolonged use. Furthermore, the electrical performance of the EGIEs under sinewave stimulation at different frequencies was also tested (Figure 3f). As the frequency decreased from 10 to 0.1 Hz, the current density output from the commercial electrodes gradually decreased, while the output current density of EGIEs closely followed the standard sinewave across all tested frequencies, which demonstrated the reliable performance of the EGIE for acquiring high-quality electrophysiological signals.

2.4. Low Noise and High Stability of EGIE in Static Physiological Signal Acquisition

An ultra-conformal bioelectronic interface can significantly enhance the signal fidelity in dynamic eletrophysiological monitoring system. The bioelectronic interface based on EGIE was prepared by first painting the precursor solution onto the epidermis, after gelation a thermoplastic polyurethane (TPU) composite layer covered with a continuous silver thin film was encapsulated onto the surface of EGIE (Figure S16, Supporting Information). We conducted a systematic study by comparing EGIEs with commercial Ag/AgCl electrodes in static ECG signal acquisition (**Figure 4a**). The ECG signals collected based on EGIEs displayed clear pulses of P wave, QRS wave, and T wave, which was equivalent to commercial Ag/AgCl electrodes. The quality of the ECG signal was evaluated by using the relative voltage ratio (T/R ratio) between the T and R peaks.[26] The observed increase of T/R ratio in EGIE primarily reflects improved signal of amplitude fidelity. Optimal T/R ratios for high-quality measurements typically fall between 0.14 and 0.5 in normal sinus rhythm, as ratios < 0.14 will increase the risk of T-wave misclassification, and ratios >0.6 may indicate pathological conditions.[27] We used EGIEs to monitor static ECG signals of different subjects. The results showed that the T/R value of EGIE was between 0.17 ± 0.02 and 0.3 ± 0.035 (Figure 4b; Figure S17, Supporting Information), which meet the requirements for high-quality monitoring of ECG signals. In addition, the sensitivity of EGIE in static ECG signal acquisition was 0.17 ± 0.02 (Figure 4b), which was higher than that of Ag/AgCl electrodes (0.14 ± 0.02), providing better fidelity signals. We also tested ECGs from EGIE with different thicknesses; the T/R ratio of the ECG signal increased as the decrease of thickness of the IEGIE (Figure S18, Supporting Information).

On the other hand, the surface electromyography (sEMG), which recorded the electrical activity of muscles from skin surface, become a promising technique in the field of human-machine interaction owing to its non-invasiveness and ease of operation. Here, the sEMG signals were recorded by the EGIE and commercial Ag/AgCl electrode (Figure 4c). The signal-to-noise ratio (SNR) of the sEMG signals recorded by the EGIE was 21.83 ± 0.12 dB, which was higher than that of the Ag/AgCl electrode (9.357 ± 0.07 dB). The baseline potential represents the noise level and can be used as another indicator of signal quality.[26a,28] As shown in Figure 4d, the root mean square (RMS) of the baseline potential recorded by the EGIE was 0.016 ± 0.0005 mV, lower than that of the Ag/AgCl electrode (0.069 ± 0.0005 mV). Even when the thickness of the EGIE reached 2.3 mm, the RMS of the baseline potential was still two times lower than that of the commercial Ag/AgCl gel electrode (Figure S19, Supporting Information). In summary, the high SNR and low baseline potential indicated that the sEMG signals recorded by the EGIE possess higher quality.

Besides, we conducted long-term testing of the EGIEs to assess their potential applications in wearable devices. In a 3-day ECG monitoring test, the EGIE did not experience detachment or damage during daily activities, and the ECG signals could be acquired with no baseline drift or peak loss throughout the entire process (Figure 4e). Figure 4f shows the sensitivity of the ECG signals recorded every day, which remained at a high level of $\approx 0.22 \pm 0.0114$. Interestingly, the ECG signals recorded by the EGIE remained stable after being reused ten times on skin, while the commercial Ag/AgCl electrode exhibited T peak loss after being reused four times (Figure S20, Supporting Information). Besides, we placed the EGIEs on the flexor carpi ulnaris (FCU) muscle belly of the subject to test long-term EMG signals. The results showed that the EGIE displayed excellent performance, maintaining an SNR level above 20 dB, while the Ag/AgCl electrode's SNR dropped to 20 dB within 6 h (Figure 4g). Significantly, the total wearing time of the long-term test exceeded 10 days, but the EGIEs did not cause any itching or irritation, demonstrating their comfort of wearing, and demonstrating the excellent long-term performance and stability of the EGIE. The stable sensing performance of EGIE was attributed to the incorporation of a supramolecular solvent system. To further evaluate the stability of EGIEs, we systematically investigated their mass variation and electrochemical impedance over time. As shown in Figure S21 (Supporting Information), the electrode mass initially decreased before stabilizing, with a 10% loss of total mass. Moreover, the impedance magnitude at 1 KHz remained remarkably stable throughout prolonged testing. This outstanding stability arises from the robust hydrogen-bonding network formed between water molecules and the abundant carboxyl/hydroxyl groups derived from citric acid and sorbitol in the supramolecular matrix. These molecular interactions significantly enhance the water retention capability of the EGIE, thereby ensuring long-term stability.

Based on the above, compared to the traditional ionogels or the PMMA-based conductive ionogels[29] (Table S1, Supporting Information), the EGIE exhibits better extensibility, anti-creep performance, lower stress relaxation, fatigue resistance under varying strains and stretching rates, and an elastic modulus closer to human skin. The measured interfacial adhesion was greater than 310 ± 15.2 N m^{-1}, and it's stable over 600 cycling test. The robust electrochemical performance of EGIE was demonstrated with a charge injection capacity after more than 10000 biphasic pulses. We also tested its biocompatibility by attaching it to skin

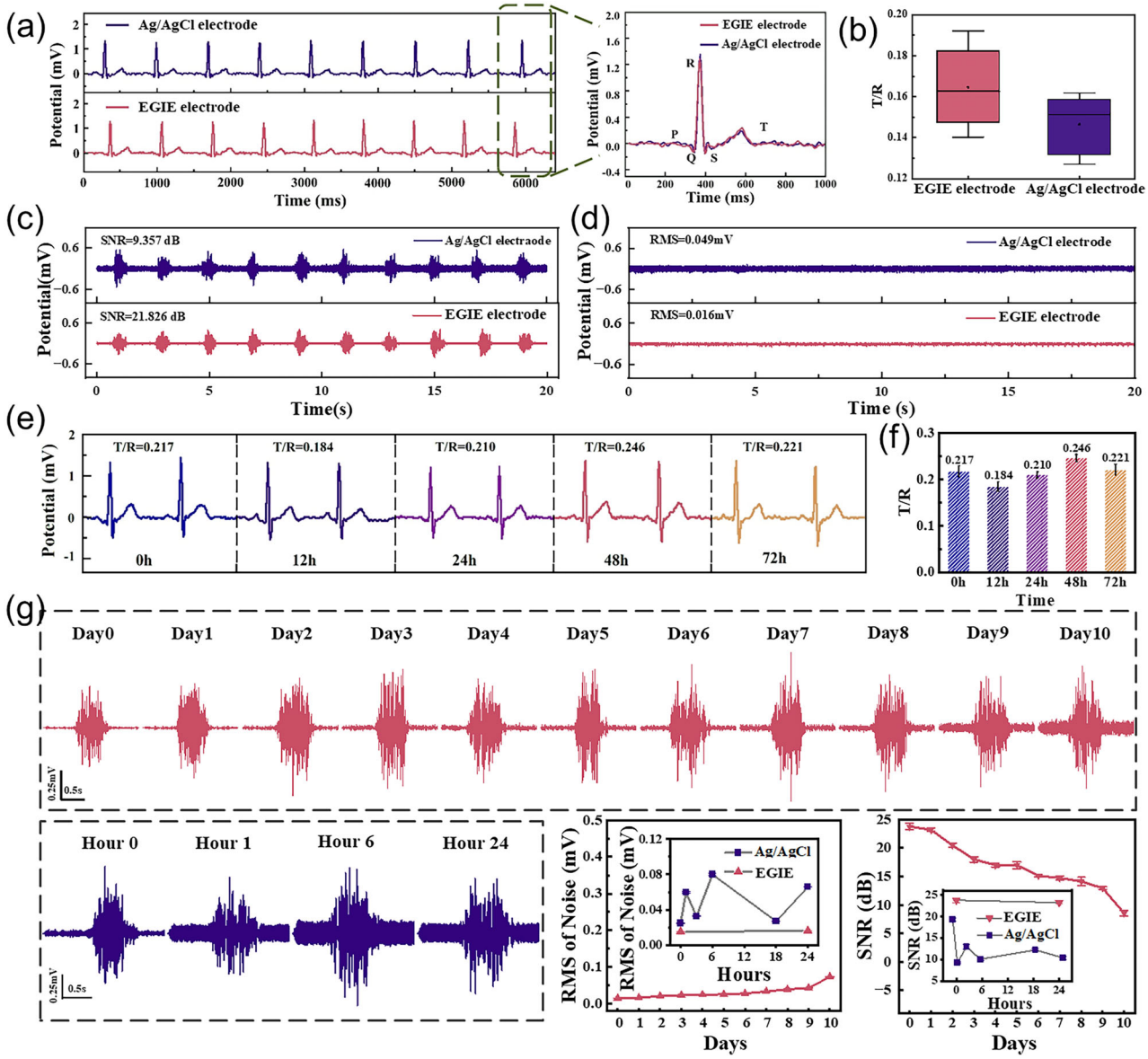

Figure 4. EGIE for Static Physiological Signal Acquisition. a) ECG signals and b) T/R values by EGIE and Ag/AgCl electrodes in static state. c) The sEMG signal baseline and RMS value of EGIE and Ag/AgCl electrodes. d) The sEMG signals and SNR value of EGIE and Ag/AgCl electrodes. e) ECG signals and f) T/R values by EGIE with 3 days. g) sEMG signals, RMS value, and SNR value recorded by EGIE and Ag/AgCl electrodes during the 10 days long-term test. Data in (G) are means ± SD, $n = 3$.

for up to seven days, observing no allergic reaction or redness. Thanks to their outstanding comprehensive performances, the EGIE achieves high-fidelity ECG signal acquisition and significantly improves the signal-to-noise ratio (SNR: 21.83 ± 0.12 dB) in EMG monitoring during dynamic motion. Notably, the EGIE maintains stable performance (SNR > 20 dB) even after 10 days of continuous wear, demonstrating its durability.

2.5. Dynamic Monitoring of Physiological Signals Using EGIE

Due to the outstanding comprehensive performances, the EGIE enables unprecedented signal fidelity during dynamic motion monitoring. Especially, the EGIE show significant advantages in ECG detection during physical activities such as walking, squatting, and jogging. In the case of these physical activities, the P-QRS-T peaks of the ECG signals by the EGIE could be clearly distinguished, while the T peak by the Ag/AgCl electrode was indistinguishable or severely disturbed due to interference from motion artifacts (**Figure 5a**; Figure S22, Supporting Information).

Sweat-induced signal degradation remains a critical limitation in wearable electrophysiology,[27c,30] causing impedance fluctuations,[27c,31] adhesion failure,[32] and motion artifact amplification. Therefore, we simulated the influence of human sweating on the EGIE performance to monitor ECG signals under static conditions. These results showed that the EGIE maintained

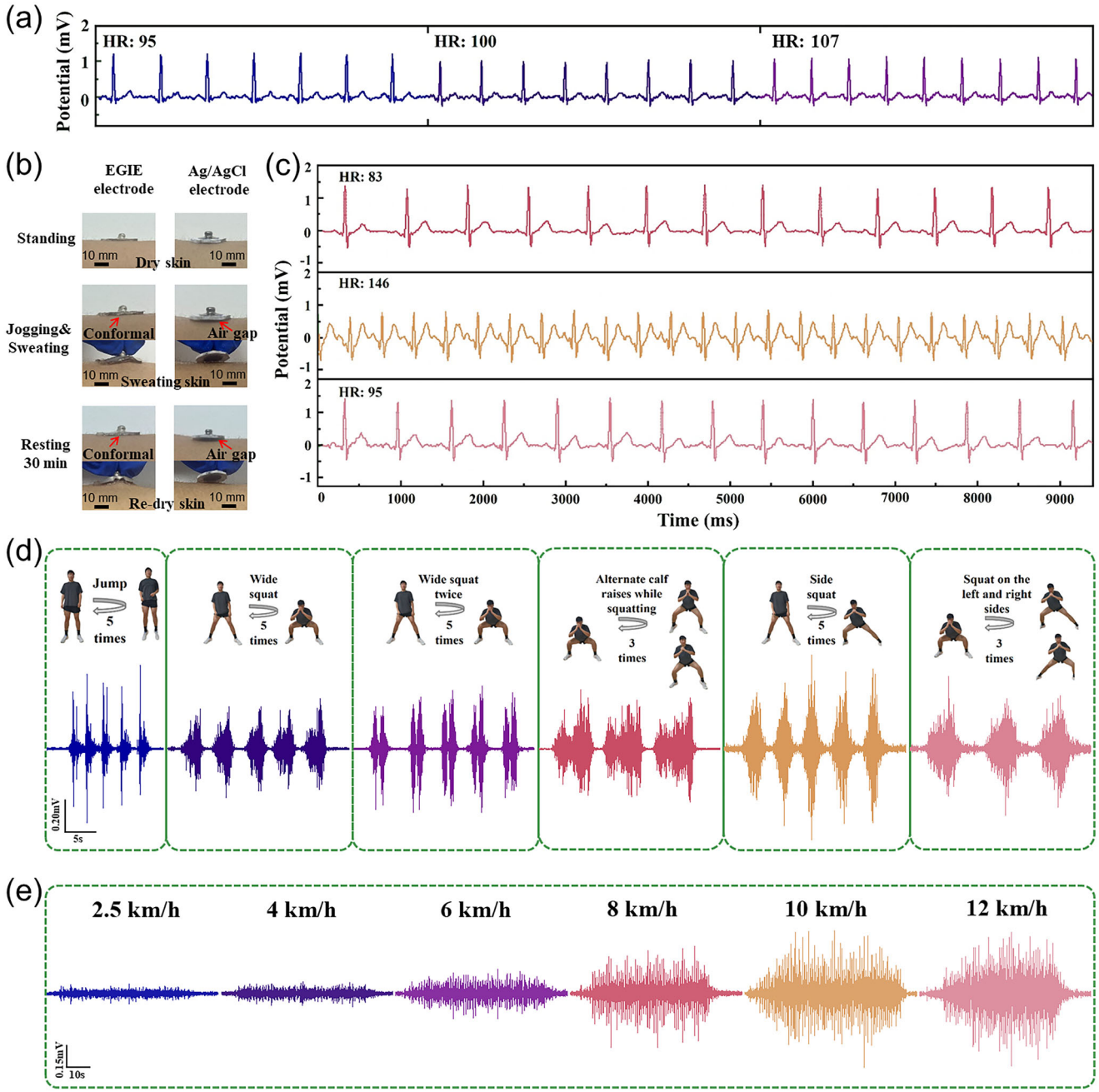

Figure 5. EGIE for Dynamic Monitoring of Physiological Signals. a) ECG signals and heart rate (HR) recorded by EGIE during physical activities such as walking, squatting, and jogging. b) Interface states between the EGIE and commercial Ag/AgCl electrode and the epidermis at different motion states: standing, jogging, and sweating, and resting for 60 min post-running. c) ECG signals and HR recorded by EGIE at different motion states from top to bottom: i) standing, ii) jogging and sweating, and iii) resting for 60 min post-running. d) EMG signals recorded by EGIE during leg stretching exercises. e) EMG signals recorded by EGIE during different running speeds.

a high-quality ECG signal output even on a wet skin surface, while the commercial Ag/AgCl electrode exhibited T peak loss (Figure S23, Supporting Information). To analyze the interfacial structure between the EGIE and epidermis, we evaluated the interfacial adhesion and impedance of the EGIE before and after artificial sweat spraying. As shown in Figure S24a (Supporting Information), the adhesion of the EGIE remained nearly unchanged after sweat exposure. Meanwhile, the skin-contact impedance of the EGIE was significantly lower than that of conventional Ag/AgCl electrodes across electrophysiological signal acquisition frequencies for both before and after sweat spraying (Figure S24b, Supporting Information). Specifically, the zwitterionic polymer in the EGIE, owing to its sulfonic acid groups, can mitigate sweat effects by forming hydrogen bonds with water molecules.[12a,27c,29e] Additionally, hydrogen bondings and electrostatic interactions between the EGIE and skin contribute to a

soft, adhesive, and conformal interface, thereby reducing interfacial impedance. These properties enable the EGIE to maintain optimal performance under sweat exposure, ensuring a stable electrode/skin interface. Based on this, we assessed the ability of EGIEs to resist sweat interference by detecting ECG signals at different dynamic states: standing, jogging and sweating, and resting for 60 min post-running. It has been found that the EGIEs could form a stable interface with the epidermis throughout the test, but the commercial Ag/AgCl electrode was easily detached from skin with high sweat content (Figure 5b). Significantly, the signals obtained by EGIEs at different states were almost unaffected by sweat; they still could provide a clear and stable P-QRS-T waveform after sweating during exercise, which showed better resistance performance to sweat than commercial Ag/AgCl electrodes (Figure 5c).

Meanwhile, the EGIE also displayed stable and distinguishable high-fidelity signal output for electromyography (EMG) detection during various complex movements. At first, we placed the EGIE on the flexor carpi ulnaris (FCU) muscle belly of the subject's arm, which successfully allow to acquire stable EMG signals from different gripping forces and various finger movements (Figure S25, Supporting Information). Next, the EGIE was placed onto the vastus lateralis muscle of the volunteer's right thigh to monitor EMG signals during leg stretching exercises. The recorded EMG signals exhibited excellent stability, and the details of each movement were clearly distinguishable (Figure 5d; Movie S3, Supporting Information). For instance, during a jump, EMG signals were clearly recorded during takeoff and landing. During squatting exercises with different speeds, the voltage amplitude of the EMG signal was varied too. Slow squatting produced a broad stimulation peak, while fast squatting resulted in sharp high peaks. Additionally, subtle motion changes also could be captured during deep squatting, such as when the toes of both feet were raised or when both legs were stretched. Furthermore, the EGIE was placed onto the long toe flexor muscle of the volunteer's right calf to monitor EMG signals during different running speeds. The EMG signals obtained at different running speeds exhibited very low baseline noise and grew progressively larger while maintaining excellent stability, as the increase of running speed (Figure 5e; Movie S4, Supporting Information). The comprehensive performance comparison under various conditions validated that EGIEs outperformed commercial electrodes in daily physiological signal monitoring, especially during monitoring daily dynamic movements.

2.6. An EGIE-Enabled ECG Wear for Multi-Parameter Physiological Monitoring

Based on the outstanding dynamic monitoring capabilities of the EGIE, we have developed a wearable multi-parameter physiological monitoring system by integrating a distributed EGIE array, an accelerometer, a temperature sensor, and a Bluetooth component on a fabric carrier (referred to as the "ECG-Wear"), as shown in **Figure 6a**. The distributed EGIE array converted the detected physiological signals into electrical signals. These signals underwent signal conditioning, processing, and transmission, and were finally sent to a microcontroller with computing and serial communication capabilities, allowing to record physiological signals during complex daily activities. Figure 6b illustrated a volunteer wearing the ECG-Wear to continuously monitor physiological signals such as 3-axis acceleration, heart rate, respiratory rate, ECG, and body temperature, during various activities including standing, elliptical trainer, chest pressing, sitting up, climbing stair, and running (Figure 6c). Due to the excellent conformal ability and interface adhesion of the EGIE, the distributed electrode array could be firmly attached to skin during movement. During various activities, the ECG-Wear could accurately and continuously monitor all physiological signals (Figure 6c; Movie S5, Supporting Information). Thanks to the exceptional mechanical, adhesive, and electrical performance of the EGIE, the multiple biological signals obtained by the ECG-Wear remained consistent and stable regardless of the activity or exercise.

In addition, we also conducted the long-term measurements for achieving real-time monitoring and acquiring high-fidelity physiological parameter by using the ECG-Wear under daily life conditions. We continuously monitored the heart rate and ECG signals of volunteers over two days of daily activities. Figures 6d shows the observed ECG signals during various normal daily activities (e.g., personal computer (PC) work, walk, sleep, experiment, and lunch) from 11:30 p.m. to 11:30 a.m. on Day 1, and from 11:30 a.m. to 11:30 p.m. on Day 2. The magnified sections in Figure 6d (i) clearly showed the ECG waveforms. We further analyzed the average heart rate during different activities, such as PC work on Day 1 [73 beats per minute (bpm)], walk (95 bpm), sleep (70 bpm) and experiment (77 bpm), as well as lunch (88 bpm), sleep (70 bpm) and walk (98 bpm) on Day 2 (Figure S26, Supporting Information). The ECG signals recorded on Day 2 also displayed similar characteristic peaks with excellent stability (Figure 6d (ii) and Figure S26, Supporting Information). It can be concluded that the ECG-Wear successfully achieved continuous high-fidelity ECG monitoring with outstanding stability for three days under daily life conditions, thanks to the excellent mechanical stability, dynamic skin conformity, stable electrical performance, and superior dynamic monitoring ability of the EGIEs. We believe that the proposed EGIE also displays potential applications in iontronic tactile sensors for achieving human-machine interaction as well as monitoring other biosignals including EEG (electroencephalogram), EOG (electro-oculogram), and EDA (Electrodermal activity).[33]

3. Conclusion

In this work, we have successfully developed a novel method for in situ formation of epidermis-gel interlocking electrode (EGIE) for detecting physiological signals during dynamic motions. The interlocking structure was formed with a self-catalytic reaction between the organogel and subcutaneous tissue. The EGIE effectively addressed several inherent challenges in dynamic monitoring of physiological signals by providing the following advantages: excellent epidermal conformability (matching the modulus of skin), outstanding mechanical stability, superior interfacial adhesion (adhesion strength >300 N m^{-1}), reliable electrochemical performance, clinical-grade biocompatibility (7-day wear without irritation). Thanks to these exceptional properties, the EGIE significantly enhanced the signal-to-noise ratio (SNR) ratio up to 21

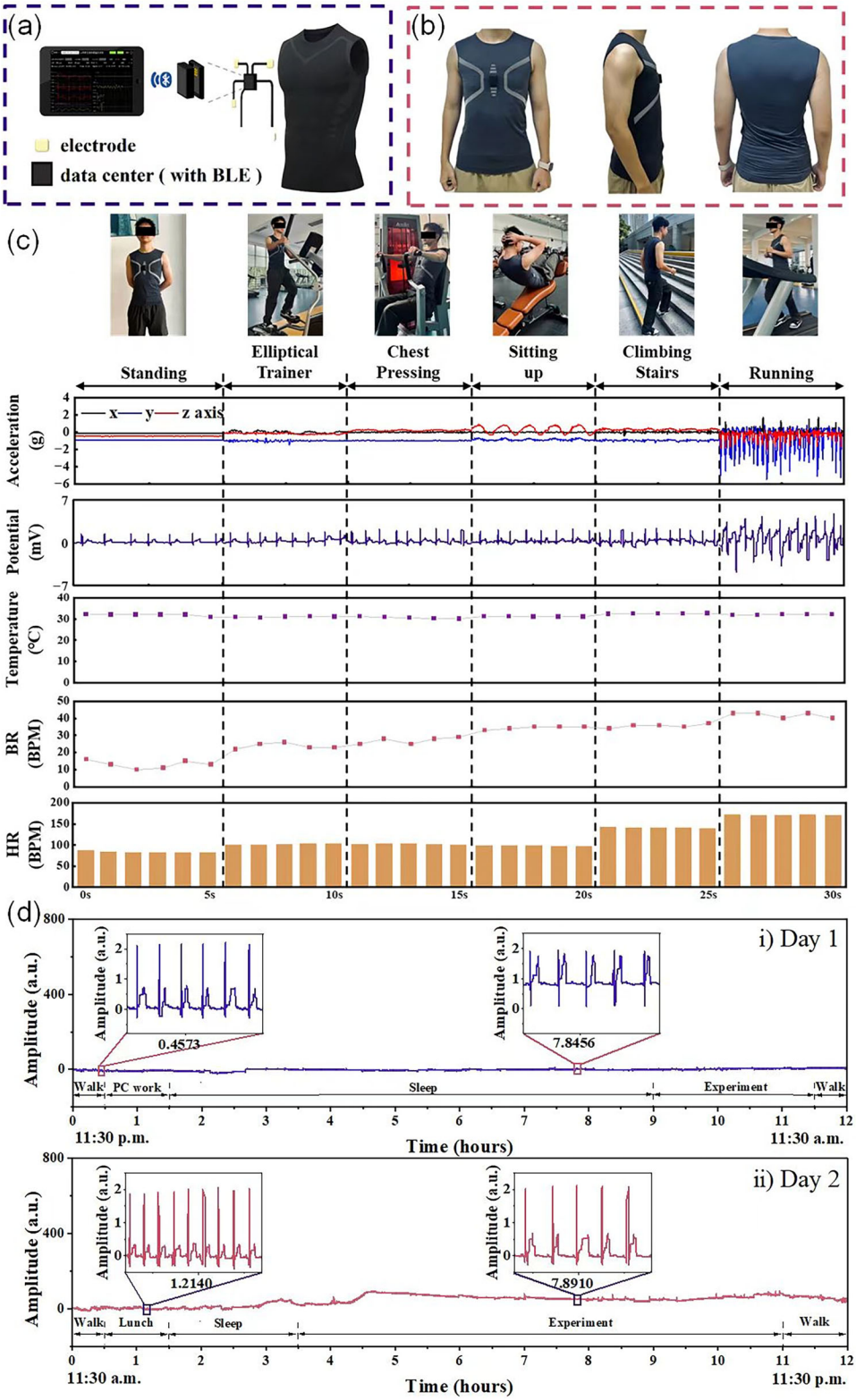

Figure 6. EGIE enabled ECG-Wear for multi-parameter physiological monitoring. a) An ECG-Wear with distributed EGIEs, sensors, and Bluetooth components on a fabric carrier. b) Human wearing the ECG-Wear. c) Multi-parameter physiological monitoring under various human motions including i) standing, ii) exercising on elliptical trainer, iii) chest pressing, iv) sitting up, v) climbing stair, and vi) running. From top to bottom: acceleration, ECG, temperature, respiratory rate, and heart rate (HR). d) Long term test of the ECG-Wear i) from 11:30 p.m. to 11:30 a.m. on Day 1, and ii) from 11:30 a.m. to 11:30 p.m. on Day 2.

dB and maintained an SNR above 20 dB even after 10 days of wear. With the superior SNR and stability, the EGIE can detect physiological signals during dynamic human motions, including ECG monitoring at walking, squatting, jogging, and post-sweating, as well as electromyogram (EMG) monitoring during leg stretching exercises and running activities. We believe that this research not only play an important role in preparing gel materials, but also can advance related fields such as skin-attachable sensor for medical diagnosis.

4. Experimental Section

Preparation of EGIE: [2-(Methacryloloxy)ethyl]dimethyl-(3-sulfopropyl) ammonium (MAEDS), 2-Acrylamido-2-methyl-1-propanesulfonic acid (AMPS), and Acrylamide (AAm) were selected as monomers, citric acid (CA) and sorbitol (Sor) as supramolecular solvent components, silver nitrate ($AgNO_3$) as the catalyst, N,N'-Methylenebisacrylamide (MBAA) as the crosslinking agent, and ammonium persulfate (APS) as the initiator. All chemical reagents were purchased from Aladdin Reagent Co., Ltd. Additionally, the commercial Ag/AgCl electrodes, commercial paste, and adhesive gel electrodes used in this study were purchased from 3M Red Dot 2223CN, GREENTEK GT20, and HDF SNJ-3, respectively. The CA/Sor supramolecular solvent (S) was prepared by ultrasonically dissolving 116.4 g of anhydrous citric acid and 144.8 g of sorbitol in 50 g of water, until fully dissolved, resulting in a uniform and transparent viscous solution. Specifically, AMPS and AAm monomers were first ultrasonically dissolved in deionized water in an ice-water bath. Then, MAEDS was added to the solution and dissolved by ultrasound. Next, the CA/Sor supramolecular solvent was added to the solution, which was sonicated in an ice-water bath and evenly dispersed for 10 min. Subsequently, MBAA, APS, and $AgNO_3$ solutions were added to the precursor solution, which was stirred thoroughly and degassed. Finally, by painting the gel precursor solution onto the epidermis, the EGIE was formed on skin within a few minutes. The detailed formulation was presented in Table S2 (Supporting Information). If not otherwise specified, the EGIEs in this study were prepared with a mole ratio of MAEDS:AMPS:AAm of 1:1:3.

Mechanical Properties Tests: Tensile strain tests for all samples were performed at room temperature using a mechanical testing machine equipped with a 50 N load cell. The reported statistics are from at least three tests on the same sample. Unless otherwise stated, standard rectangular test specimens (length ≈ 30–40 mm, width ≈ 10 mm) were clamped on a tensile stage and stretched at a tensile speed of 50 mm/min. Step loading-unloading tests were performed with multiple strains of 50%, 100%, 200%, 300%, 400% and 500%. Creep resistance was tested by applying a load of 0.2 N to the sample and measuring its deformation change with time under this load. Stress relaxation experiments were performed by stretching the sample to 100% strain and then measuring its stress change with time under this strain. Fatigue resistance tests were performed by stretching the sample to different strains (25%, 50%, 100%, 250%, 500% strain) at a tensile speed of 1 Hz and performing 1000 cycles of loading-unloading tests.

Interface Adhesion Tests: The adhesion force of the EGIE was measured using a 180° peel test on a mechanical testing machine. Plasma-treated PET film was used as the substrate. A EGIE film was formed on the substrate, and another plasma-treated substrate was placed on top. The sample dimensions were 8–10 mm in width and 60–80 mm in length. A load-displacement curve test was performed using a tensile fixture at a peel test speed of 50 mm min^{-1}. The adhesion force was determined by calculating the average peel force (F) and dividing it by the sample width (w). To evaluate the adhesion stability of the EGIE, tensile testing was conducted. A hydrophilic PMMA probe (10 × 10 mm) was attached to the mechanical testing machine's fixture. The probe was pressed onto the EGIE film at a constant speed of 10 μm s^{-1} until the contact force reached 1 N. This position was held for 5 s, followed by detachment from the material's surface at the same constant speed of 10 μm s^{-1}. The corresponding adhesion-detachment behavior curve was obtained. The adhesion strength of the EGIE was calculated as the ratio of the peak peel force to the PMMA probe's surface area.

Electrochemical Properties Tests: For characterizing the impedance performance of EGIE with different mole ratio, an electrochemical workstation (CHI660E, Shanghai Chenhua Apparatus Shanghai Chenhua Co., Ltd.) was used. In the electrochemical impedance spectroscopy, the measurement frequency range was 20 Hz–150 kHz, a sine wave current with an amplitude of 5 mV was used, and the test voltage was the open circuit voltage. When characterizing the electrochemical stability, the EGIEs were connected in series with a signal generator (AFG1022, Tektronix) to provide symmetrical two-phase voltage pulses (100 ms pulse width, 10 Hz pulse frequency, voltage input ±500 mV) between the pathways, and a digital oscilloscope (TPS2012B, Tektronix) was used to receive the signals.

In Vitro Biocompatibility Assessment of EGIEs: For cell imaging protocol, L929 cells were cultured in MEM medium within 24-well plates for imaging and viability assays. The study comprised two groups. For the Control: 1000 μL per well complete medium, and the EGIE: 1000 μL per well electrode extract (prepared by UV-sterilizing 8-mm diameter electrodes for 60 min per side, followed by 24-h immersion in complete medium at 1 piece/mL). Log-phase L929 cells were counted, diluted 1:50, and seeded at 1×10^5 cells per dish in confocal dishes. After 24-h incubation (5% CO_2, 37 °C), cells were rinsed with PBS to remove serum residuals, stained with fluorescent dye (1 mL per dish, 15 min, dark), and imaged at 100 × magnification after three PBS washes.

For cell viability assay (MTT), Log-phase L929 cells were seeded at 2×10^4 cells per well in 24-well plates and cultured overnight (5% CO_2, 37 °C). Treatment groups included the Control: 1000 μL/well complete medium, and the EGIE: 1000 μL per well electrode extract. After 144-h incubation, cultures were replaced with MTT-containing medium (0.5 mg per mL, 1000 μL per well, 4 h). Formazan crystals were dissolved in DMSO (100 μL per well, 10 min shaking), and absorbance at 570 nm was measured. Relative viability (%) was calculated as:

$$Viability = \frac{(OD_{sample} - OD_{blank})}{(OD_{control} - OD_{blank})} \times 100\% \quad (1)$$

where OD_{blank} represents DMSO-only absorbance.

Monitoring of ECG/EMG Signals: To assess the bioelectric communication performance at the tissue-electrode interface, the EGIE was used to record electrocardiogram (ECG) and electromyogram (EMG) signals. For ECG monitoring, three electrodes were placed on the left forearm, right forearm, and left abdomen. The ECG signals were recorded using an electrocardiograph (PC-80B, Heal Force). For EMG monitoring, three electrodes were positioned at the ends of the flexor carpi ulnaris (FCU) muscle on the forearm and near the elbow. The EMG signals were generated by gripping rings of varying weights to stimulate muscle activity. Commercial Ag/AgCl electrodes were also used for comparison with the EGIEs. EMG signals were recorded using the same digital oscilloscope (TBS 1152B, Tektronix). For ECG-Wear monitoring system, the distributed EGIE array was strategically positioned on specific areas of the body, including both sides of the chest, the right abdomen, and both sides of the waist. Once the ECG-Wear was worn, the silver electrodes embedded in the garment were closely adhered to the EGIE array, ensuring stable contact. Subsequently, the communication accessory was connected to the ECG-Wear, and the switch was activated until the green indicator light turns on. The data acquisition device was then powered on and connected to the ECG-Wear via Bluetooth. Upon establishing a successful connection, data collection can be initiated, enabling real-time monitoring of multiple physiological parameters from the body surface.

Statistical Analysis: All experiments in this paper were repeated three times, and the experimental results were processed by statistical methods. All results are presented as the mean ± standard deviation (SD). Data distribution was assumed to be normal for all parametric tests, but not formally tested, and no significant difference analysis was performed. The processed data were plotted using Origin software.

Supporting Information

Supporting Information is available from the Wiley Online Library or from the author.

Acknowledgements

This work was supported by National key R&D project from Minister of Science and Technology, China (2024YFE0200900), National Natural Science Foundation of China (62371298), the Science and Technology Innovation Council of Shenzhen under grants KQTD20170810105439418, the talent development funding of Fujian Normal University (Grant No. Y072R001K13).

Conflict of Interest

The authors declare no conflict of interest.

Author Contributions

C.H. and J.Z. contributed equally to this work. C.B.H. and J.Z. conceived the idea, designed and conducted the experiments, and drafted the manuscript. J.X., W.H.Z., M.Y.X., and Z.H.L. prepared the materials and conducted the experiments. D.W., H.Y.Z., and Z.N.G. were responsible for ECG and EMG signal acquisition. J.Z. and Y.F.L. prepared the ECG-Wear. H.F.W. supervised the experimental work and edited the manuscript. G.H.L. reviewed and edited the manuscript. Z.C.P. was responsible for the entire project management and fundraising.

Data Availability Statement

The data that support the findings of this study are available in the supplementary material of this article.

Keywords

bioelectronic interface, Electrophysiological signals, epidermal electrodes, long-term stability, reliable monitoring

Received: April 14, 2025
Revised: June 29, 2025
Published online:

[1] a) Y. Chen, Y. Zhang, Z. Liang, Y. Cao, Z. Han, X. Feng, *npj Flexible Electron.* **2020**, *4*, 2; b) W. Li, Y. Li, Z. Song, Y.-X. Wang, W. Hu, *Chem. Soc. Rev.* **2024**, *53*, 10575; c) H. Wang, G. Lin, Y. Lin, Y. Cui, G. Chen, Z. Peng, *J. Colloid Interface Sci.* **2024**, *668*, 142.

[2] a) W. Gao, S. Emaminejad, H. Y. Y. Nyein, S. Challa, K. Chen, A. Peck, H. M. Fahad, H. Ota, H. Shiraki, D. Kiriya, D.-H. Lien, G. A. Brooks, R. W. Davis, A. Javey, *Nature* **2016**, *529*, 509; b) S. Zheng, W. Li, Y. Ren, Z. Liu, X. Zou, Y. Hu, J. Guo, Z. Sun, F. Yan, *Adv. Mater.* **2022**, *34*, 2106570; c) J. Liu, W. Zhao, Z. Ma, H. Zhao, L. Ren, *Mater. Today* **2024**, *81*, 84; d) G. Tian, W. Deng, T. Yang, J. Zhang, T. Xu, D. Xiong, B. Lan, S. Wang, Y. Sun, Y. Ao, L. Huang, Y. Liu, X. Li, L. Jin, W. Yang, *Adv. Mater. 36*, 2313612; e) Z. Wang, X. Zhao, K. Yan, P. Zhang, S. Zhang, H. Fan, *Mater. Sci. Eng.: R: Rep.* **2025**, *164*, 100987.

[3] a) H. Yuk, B. Lu, X. Zhao, H. bioelectronics, *Chem. Soc. Rev.* **2019**, *48*, 1642; b) W. Gao, C. Yu, *Adv. Healthcare Mater.* **2021**, *10*, 2101548.

[4] a) M. Yang, P. Chen, X. Qu, F. Zhang, S. Ning, L. Ma, K. Yang, Y. Su, J. Zang, W. Jiang, T. Yu, X. Dong, Z. Luo, *ACS Nano* **2023**, *17*, 885; b) V. Timosina, T. Cole, H. Lu, J. Shu, X. Zhou, C. Zhang, J. Guo, O. Kavehei, S.-Y. Tang, *Biosens. Bioelectron.* **2023**, *235*, 115414; c) X. Du, L. Yang, X. Shi, C. Ye, Y. Wang, D. Song, W. Xiong, X. Gu, C. Lu, N. Liu, *ACS Nano* **2024**, *18*, 34971.

[5] a) S. Lee, B. Ozlu, T. Eom, D. C. Martin, B. S. Shim, *Biosens. Bioelectron.* **2020**, *170*, 112620; b) J. H. Koo, J.-K. Song, D.-H. Kim, D. Son, *ACS Mater. Lett.* **2021**, *3*, 1528; c) B. Song, X. Fan, J. Shen, H. Gu, *Chem. Eng. J.* **2023**, *474*, 145780; d) X. Qu, Q. Wang, D. Gan, H. Sun, Z. Ni, X. Dong, *Nano Lett.* **2025**, *25*, 4759.

[6] a) M. Yuan, Y. Long, T. Liu, J. Liu, S. Qiu, T. Lin, F. Xu, Y. Fang, *Mater. Today* **2024**, *75*, 166; b) J. Dong, J. Hou, Y. Peng, Y. Zhang, H. Liu, J. Long, S. Park, T. Liu, Y. Huang, *Adv. Mater.* **2024**, *36*, 2409071; c) B. Park, C. Jeong, J. Ok, T.-i. Kim, *Chem. Rev.* **2024**, *124*, 6148.

[7] a) D. Won, J. Bang, S. H. Choi, K. R. Pyun, S. Jeong, Y. Lee, S. H. Ko, *Chem. Rev.* **2023**, *123*, 9982; b) K. K. Kim, M. Kim, K. Pyun, J. Kim, J. Min, S. Koh, S. E. Root, J. Kim, B.-N. T. Nguyen, Y. Nishio, S. Han, J. Choi, C. Y. Kim, J. B. H. Tok, S. Jo, S. H. Ko, Z. Bao, *Nat. Electron.* **2023**, *6*, 64; c) Y. Jung, K. R. Pyun, S. Yu, J. Ahn, J. Kim, J. J. Park, M. J. Lee, B. Lee, D. Won, J. Bang, S. H. Ko, *Nano-Micro Lett.* **2025**, *17*, 127.

[8] a) S. J. K. O'Neill, Z. Huang, M. H. Ahmed, A. J. Boys, S. Velasco-Bosom, J. Li, R. M. Owens, J. A. McCune, G. G. Malliaras, O. A. Scherman, *Adv. Mater.* **2023**, *35*, 2207634; b) P. Tan, H. Wang, F. Xiao, X. Lu, W. Shang, X. Deng, H. Song, Z. Xu, J. Cao, T. Gan, B. Wang, X. Zhou, *Nat. Commun.* **2022**, *13*, 358.

[9] a) Y. Zhao, S. Zhang, T. Yu, Y. Zhang, G. Ye, H. Cui, C. He, W. Jiang, Y. Zhai, C. Lu, X. Gu, N. Liu, *Nat. Commun.* **2021**, *12*, 4880; b) L. Eskandarian, E. Pajootan, A. Toossi, H. E. Naguib, *Adv. Fiber Mater.* **2023**, *5*, 819.

[10] D. Won, H. Kim, J. Kim, H. Kim, M. W. Kim, J. Ahn, K. Min, Y. Lee, S. Hong, J. Choi, C. Y. Kim, T.-S. Kim, S. H. Ko, *Nat. Electron.* **2024**, *7*, 475.

[11] H. Yoon, J. Choi, J. Kim, J. Kim, J. Min, D. Kim, S. Jeong, J. G. Lee, J. Bang, S. H. Choi, Y. Jeong, C.-Y. Kim, S. H. Ko, *Adv. Funct. Mater.* **2024**, *34*, 2313504.

[12] a) X. Shi, D. Song, W. Hu, C. Li, W. Zhang, S. Wang, Q. Hu, Y. Wang, X. Wang, Y. Zhang, B. Peng, Z. Wang, N. Liu, *Adv. Funct. Mater.* **2024**, *34*, 2314775; b) H. Tang, Y. Li, B. Chen, X. Chen, Y. Han, M. Guo, H.-q. Xia, R. Song, X. Zhang, J. Zhou, *ACS Nano* **2022**, *16*, 17931.

[13] a) X. Liang, L. Li, Y. Liu, D. Chen, X. Wang, S. Hu, J. Wang, H. Zhang, C. Sun, C. Liu, *Comput. Biol. Med.* **2022**, *145*, 105445; b) Y. Li, W. Liu, Y. Deng, W. Hong, H. Yu, *npj Flexible Electron.* **2021**, *5*, 3.

[14] a) S. Shukla, S. A. Machekposhti, N. Joshi, P. Joshi, R. J. Narayan, *Small Sci.* **2023**, *3*, 2200087; b) C. Wang, Y. Yang, J. Zhang, H. Zhang, Q. Wang, S. Ma, P. Zhao, Z. Li, Y. Liu, *Adv. Sci.* **2025**, *12*, 2412140.

[15] P. Won, J. J. Park, T. Lee, I. Ha, S. Han, M. Choi, J. Lee, S. Hong, K.-J. Cho, S. H. Ko, *Nano Lett.* **2019**, *19*, 6087.

[16] H. Kim, J. Lee, U. Heo, D. K. Jayashankar, K.-C. Agno, Y. Kim, C. Y. Kim, Y. Oh, S.-H. Byun, B. Choi, H. Jeong, W.-H. Yeo, Z. Li, S. Park, J. Xiao, J. Kim, J.-W. Jeong, *Sci. Adv.* **2024**, *10*, adk5260.

[17] F. Liu, Y. Chen, Y. Huang, Y. Li, Z. Lu, H. Han, X. Song, Q. Jin, J. Ji, *Nat. Commun.* **2024**, *15*, 9004.

[18] a) J. Gao, M. Hu, H. Sun, Y. Wang, Y. Wei, W. Li, L. Zheng, M. Xu, Q. Lu, Z. Liu, H. Yang, Y. Wang, W. Song, X. Wang, W. Huang, *npj Flexible Electron.* **2025**, *9*, 6; b) S. Afewerki, X. Wang, G. U. Ruiz-Esparza, C.-W. Tai, X. Kong, S. Zhou, K. Welch, P. Huang, R. Bengtsson, C. Xu, M. Strømme, *ACS Nano* **2020**, *14*, 17004; c) Z. Wu, Y. Hong, *ACS Appl. Mater. Interfaces* **2019**, *11*, 33734.

[19] a) C. Wang, H. Wang, B. Wang, H. Miyata, Y. Wang, M. O. G. Nayeem, J. J. Kim, S. Lee, T. Yokota, H. Onodera, T. Someya, *Sci. Adv.* **2022**, *8*, abo1396; b) Z. Zhang, J. Yang, H. Wang, C. Wang, Y. Gu, Y. Xu, S. Lee, T. Yokota, H. Haick, T. Someya, Y. Wang, *Sci. Adv.* **2024**, *10*, adj5389;

c) M. Xia, J. Liu, B. J. Kim, Y. Gao, Y. Zhou, Y. Zhang, D. Cao, S. Zhao, Y. Li, J.-H. Ahn, *Adv. Sci.* **2024**, *11*, 2304871.

[20] a) S. Zhang, M. Sharifuzzamn, S. M. S. Rana, M. A. Zahed, S. Sharma, Y. Shin, H. Song, J. Y. Park, *Nano Res.* **2023**, *16*, 7627; b) D. Clausen, T. Stuart, K. A. Kasper, T. D. McGuire, J. P. Dabdoub, A. Russell, D. Perez, V. Sathishkumaraselvam, A. Miller, S. Roberts, P. Gutruf, *Adv. Funct. Mater.* **2025**, *35*, 2407086.

[21] a) J. Deng, H. Yuk, J. Wu, C. E. Varela, X. Chen, E. T. Roche, C. F. Guo, X. Zhao, *Nat. Mater.* **2021**, *20*, 229; b) X. Lin, Z. Ou, X. Wang, C. Wang, Y. Ouyang, I. M. Mwakitawa, F. Li, R. Chen, Y. Yue, J. Tang, W. Fang, S. Chen, B. Guo, J. Ouyang, T. Shumilova, Y. Zhou, L. Wang, C. Zhang, K. Sun, *Interdisciplin. Mater.* **2024**, *3*, 775; c) X. Wang, W. Qiu, C. Lu, Z. Jiang, C. Hou, Y. Li, Y. Wang, H. Du, J. Zhou, X. Y. Liu, *Adv. Funct. Mater.* **2024**, *34*, 2311535.

[22] Y. Zhao, S. Song, X. Ren, J. Zhang, Q. Lin, Y. Zhao, *Chem. Rev.* **2022**, *122*, 5604.

[23] a) H. Ji, X. Song, H. Cheng, L. Luo, J. Huang, C. He, J. Yin, W. Zhao, L. Qiu, C. Zhao, *ACS Appl. Mater. Interfaces* **2020**, *12*, 31079; b) Y. Liu, L. Wang, J. Jiang, X. Wang, C. Dai, G. Weng, *Macromolecules* **2023**, *56*, 49.

[24] A. L. Lakela, E. Berntsson, F. Vosough, J. Jarvet, S. Paul, A. Barth, A. Gräslund, P. M. Roos, S. K. T. S. Wärmländer, *Sci. Rep.* **2025**, *15*, 5439.

[25] a) P. Cai, C. Wan, L. Pan, N. Matsuhisa, K. He, Z. Cui, W. Zhang, C. Li, J. Wang, J. Yu, M. Wang, Y. Jiang, G. Chen, X. Chen, *Nat. Commun.* **2020**, *11*, 2183; b) X. Li, L. He, Y. Li, M. Chao, M. Li, P. Wan, L. Zhang, *ACS Nano* **2021**, *15*, 7765; c) L. Lan, J. Ping, H. Li, C. Wang, G. Li, J. Song, Y. Ying, *Adv. Mater.* **2024**, *36*, 2401151; d) S. Wang, Y. Nie, H. Zhu, Y. Xu, S. Cao, J. Zhang, Y. Li, J. Wang, X. Ning, D. Kong, *Sci. Adv.* **2022**, *8*, abl5511; e) A. Inoue, H. Yuk, B. Lu, X. Zhao, *Sci. Adv.* **2020**, *6*, aay5394.

[26] a) H. Lai, Y. Liu, Y. Cheng, L. Shi, R. Wang, J. Sun, *Adv. Sci.* **2023**, *10*, 2300793; b) A. J. Dunn, M. H. ElRefai, P. R. Roberts, S. Coniglio, B. M. Wiles, A. B. Zemkoho, *Artif. Intell. Med.* **2021**, *119*, 102139; c) Z. Wu, T. Qian, S. Li, N. Wang, T. Zhou, X. Yuan, *Sens. Actuators, A* **2024**, *379*, 115912; d) Y. Ding, Y. Shi, D. Yu, W. Wang, *Colloids Surf. A* **2023**, *675*, 132060; e) Z. Wu, T. Qian, S. Zhao, T. Zhou, *Sens. Actuators, A* **2025**, *387*, 116400.

[27] a) P. L. Leif Sörnmo, *Bioelectrical Signal Processing in Cardiac and Neurological Applications (Biomedical Engineering)*, Elsevier, Amsterdam, Netherlands, **2005**; b) L. Meng, Q. Fu, S. Hao, F. Xu, J. Yang, *Chem. Eng. J.* **2022**, *427*, 131999; c) H. Yang, S. Ji, I. Chaturvedi, H. Xia, T. Wang, G. Chen, L. Pan, C. Wan, D. Qi, Y.-S. Ong, X. Chen, *ACS Mater. Lett.* **2020**, *2*, 478; d) D. K. Bloomfield, R. Ziegler, *J. Electrocardiol.* **1969**, *2*, 167; e) M. ElRefai, M. Abouelasaad, B. M. Wiles, A. J. Dunn, S. Coniglio, A. B. Zemkoho, P. R. Roberts, *J. Intervent. Cardiac Electrophysiol.* **2022**, *65*, 1245.

[28] a) M. Correa, M. Projetti, I. A. Siegler, N. Vignais, *Sensors* **2023**, *23*, 7969; b) G. Tian, D. Yang, C. Liang, Y. Liu, J. Chen, Q. Zhao, S. Tang, J. Huang, P. Xu, Z. Liu, D. Qi, *Adv. Mater.* **2023**, *35*, 2212302.

[29] a) G. Li, Z. Deng, M. Cai, K. Huang, M. Guo, P. Zhang, X. Hou, Y. Zhang, Y. Wang, Y. Wang, X. Wu, C. F. Guo, *npj Flexible Electron.* **2021**, *5*, 23; b) W. Liu, R. Xie, J. Zhu, J. Wu, J. Hui, X. Zheng, F. Huo, D. Fan, *npj Flexible Electron.* **2022**, *6*, 68; c) H. Ye, B. Wu, S. Sun, P. Wu, *Nat. Commun.* **2024**, *15*, 885; d) Y. Liu, C. Wang, J. Xue, G. Huang, S. Zheng, K. Zhao, J. Huang, Y. Wang, Y. Zhang, T. Yin, Z. Li, *Adv. Healthcare Mater.* **2022**, *11*, 2200653; e) C. Sun, J. Luo, T. Jia, C. Hou, Y. Li, Q. Zhang, H. Wang, *Chem. Eng. J.* **2022**, *431*, 134012; f) M. Zheng, L. Li, X. Ye, Z. Ji, Y. Wang, Z. Wang, S. Lin, M. Wang, W. Yan, J. Yang, P. Zhou, Y. Zhang, R. Niu, H. Haick, Y. Wang, *Chem. Eng. J.* **2025**, *512*, 162451; g) S. Tang, D. Sha, Z. He, X. Chen, Y. Ma, C. Liu, Y. Yuan, *Adv. Healthcare Mater.* **2023**, *12*, 2300475; h) R. Chen, L. Wang, D. Ji, M. Luo, Z. Zhang, G. Zhao, X. Chang, Y. Zhu, *Carbohydr. Polym.* **2025**, *352*, 123220; i) G. J. Rodriguez-Rivera, A. Post, M. John, D. Bashe, F. Xu, T. Larue, A. Nkansah, M. Wancura, M. Chwatko, C. Waldron, N. Kalkunte, J. Zoldan, M. Arseneault, A. Elgalad, M. K. Rausch, M. Razavi, E. Cosgriff-Hernandez, *Biomaterials* **2025**, *317*, 123071; j) Y. M. Kim, H. C. Moon, *Adv. Funct. Mater.* **2020**, *30*, 1907290; k) J. Song, R. Yang, J. Shi, X. Chen, S. Xie, Z. Liao, R. Zou, Y. Feng, T. T. Ye, C. F. Guo, *Sci. Adv.* **2025**, *11*, adu6086; l) Y. He, Y. Cheng, C. Yang, C. F. Guo, *Nat. Mater.* **2024**, *23*, 1107; m) Y. Jiang, A. A. Trotsyuk, S. Niu, D. Henn, K. Chen, C.-C. Shih, M. R. Larson, A. M. Mermin-Bunnell, S. Mittal, J.-C. Lai, A. Saberi, E. Beard, S. Jing, D. Zhong, S. R. Steele, K. Sun, T. Jain, E. Zhao, C. R. Neimeth, W. G. Viana, J. Tang, D. Sivaraj, J. Padmanabhan, M. Rodrigues, D. P. Perrault, A. Chattopadhyay, Z. N. Maan, M. C. Leeolou, C. A. Bonham, S. H. Kwon, et al., *Nat. Biotechnol.* **2023**, *41*, 652; n) S. J. K. O'Neill, M. Ashizawa, A. M. McLean, R. R.-M. Serrano, T. Shimura, M. Agetsuma, M. Tsutsumi, T. Nemoto, C. D. J. Parmenter, J. A. McCune, G. G. Malliaras, N. Matsuhisa, O. A. Scherman, *Adv. Mater.* **2025**, *37*, 2415687.

[30] a) A. Akhtar, J. Sombeck, B. Boyce, T. Bretl, *Sci. Rob.* **2018**, *3*, aap9770; b) H. Ma, Z. Liu, X. Lu, S. Zhang, C. Tang, Y. Cheng, H. Zhang, G. Liu, C. Sui, C. Ding, R. Yang, T. Luo, *Acta Biomater.* **2024**, *187*, 183; c) S. Harimurti, W. Wang, K. Sasaki, C. Okuda, T. Jonathan Wijaya, M. Osman Goni Nayeem, S. Lee, T. Yokota, T. Someya, *Mater. Today* **2024**, *74*, 94; d) Y. Wang, H. Haick, S. Guo, C. Wang, S. Lee, T. Yokota, T. Someya, *Chem. Soc. Rev.* **2022**, *51*, 3759.

[31] J. Li, Z. Liu, Y. Tang, J. Xian, C. He, H. Wu, M. Liu, F. Li, *CCS Chemistry* **2024**, *6*, 450.

[32] a) N. Rodeheaver, H. Kim, R. Herbert, H. Seo, W.-H. Yeo, Breathable, W., *ACS Appl. Electron. Mater.* **2022**, *4*, 503; b) J. Luo, C. Sun, B. Chang, B. Zhang, K. Li, Y. Li, Q. Zhang, H. Wang, C. Hou, *Adv. Funct. Mater.* **2024**, *34*, 2400884; c) L. Zhang, K. S. Kumar, H. He, C. J. Cai, X. He, H. Gao, S. Yue, C. Li, R. C.-S. Seet, H. Ren, J. Ouyang, *Nat. Commun.* **2020**, *11*, 4683.

[33] a) Y. Cheng, C. Guo, S. Li, K. Deng, J. Tang, Q. Luo, S. Zhang, Y. Chang, T. Pan, *Adv. Funct. Mater.* **2022**, *32*, 2205947; b) Y. Chang, L. Wang, R. Li, Z. Zhang, Q. Wang, J. Yang, C. F. Guo, T. Pan, *Adv. Mater.* **2021**, *33*, 2003464; c) Y. Li, N. Bai, Y. Chang, Z. Liu, J. Liu, X. Li, W. Yang, H. Niu, W. Wang, L. Wang, W. Zhu, D. Chen, T. Pan, C. F. Guo, G. Shen, *Chem. Soc. Rev.* **2025**, *54*, 4651.